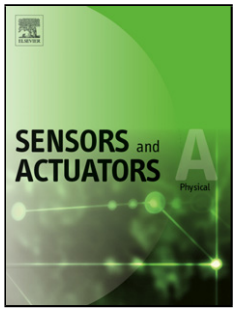

Title: Sensing System for Salinity Testing Using Laser-induced Graphene Sensors

Authors: Anindya Nag, Subhas Chandra Mukhopadhyay, J*ü*rgen Kosel

PII: S0924-4247(17)30974-3
DOI: http://dx.doi.org/doi:10.1016/j.sna.2017.08.008
Reference: SNA 10262

To appear in: *Sensors and Actuators A*

Received date: 24-5-2017
Revised date: 2-8-2017
Accepted date: 2-8-2017

Please cite this article as: Anindya Nag, Subhas Chandra Mukhopadhyay, J*ü*rgen Kosel, Sensing System for Salinity Testing Using Laser-induced Graphene Sensors, Sensors and Actuators: A Physicalhttp://dx.doi.org/10.1016/j.sna.2017.08.008

Sensing System for Salinity Testing Using Laser-induced Graphene Sensors

Anindya Nag[1*], Subhas Chandra Mukhopadhyay[1], Jürgen Kosel[2]

[1]Faculty of Science and Engineering Macquarie University Sydney, NSW, Australia.

[2]Computer, Electrical and Mathematical Sciences & Engineering Division
King Abdullah University of Science and Technology (KAUST)
Saudi Arabia.

*Corresponding author email: anindya1991@gmail.com

Highlights:

- A low-cost salinity system was developed and implemented.
- Laser ablated graphene was formed from commercial polyimide films.
- The photo-thermally induced graphene was transferred to Kapton tapes to form sensor patches.
- Salt samples with different concentrations were tested with these sensor patches via serial dilution.
- A microcontroller based system was formed to enhance the signal conditioning circuit.

Abstract— **The paper presents the development and implementation of a low-cost salinity sensing system. Commercial polymer films were laser ablated at specific conditions to form graphene-based sensors on flexible Kapton substrates. Sodium chloride was considered as the primary constituent for testing due to its prominent presence in water bodies. The sensor was characterized by testing different concentrations of sodium chloride. A standard curve was developed to perform real-time testing with a sample taken from sea water of unknown concentration. The sensitivity and resolution of these graphene sensors for the experimental solutions were 1.07 Ω/ppm and 1 ppm respectively. The developed system was validated by testing it with a real sample and cross checking it on the calibration curve. The signal conditioning circuit was further enhanced by embedding a microcontroller to the designed system. The obtained results did provide a platform for implementation of a low-cost salinity sensing system that could be used in marine applications.**

Keywords— Graphene; Polyimide; Laser-induced; Salt concentration; Salinity measurement.

1. Introduction

Sea water, as we see it consists of different elements sustaining plant and animal life. Each constituent has a certain effect on the life-sustaining inside it. One of them is the effect of salinity on the marine life [1, 2]. Salinity can be defined as the amount of salt present in the water bodies like sea and rivers. It is expressed by electrical conductivity per unit distance (µS/cm) at a particular temperature. There are ongoing studies to determine the effects caused by the change in salinity level in the water bodies. Rise in temperature, oil spills in water bodies, discharging of waste materials and climate changes are some of the common reasons for the change of its levels. The effects of the rise of salinity in sea water are detrimental to plants. The growth of plants and seed germination is affected by even slight changes in the salt concentration. Higher levels of salinity can cause difficulty in extracting water from the soil. This can be toxic to plants. A small increase in salinity increases the density of the water bodies like rivers, thus, sinking it to the bottom and floating across the river basins. Currently, a lot of research work [3-6] is going on to determine the optimum concentration of salinity in sea water. It is expensive to remove the excess salt from sea water due to the high-quality equipment needed to extract the salt. The Murray-Darling Basin report 2015-16 [7] showed that around 524,728 tons of salt water

were removed from River Murray, Australia in one year. This is an alarming rate considering the amount of salt present in just one water body.

There has been some research done [8-16] on the monitoring and evaluation of salinity monitoring systems. Certain disadvantages attached to each developed technique make them inefficient to use on an industrial scale. Optical sensors used for salinity testing [8] measures a concentration of 200 mM to 2M. Apart from the higher initial cost of fabrication of the sensor developed with the chloride-quenchable fluorescent probe, the sensor does not measure small changes, i.e., it has a small sensitivity. Other techniques involve the use of SMOS satellites developed by NASA [9] for soil moisture and ocean salinity testing. Even though this technique would be much more accurate than the previous one, the infrastructure cost is high which would be difficult to maintain if applied to smaller water bodies. Grating sensors for salinity and temperature measurements made of acrylate and polyimide coated fibers for testing the sensor at Bragg's wavelength have also been developed [10]. The biggest disadvantage of using a coating on the fibers is it is inefficient to be re-used. Thus, it is a state-of-art to develop a low-cost, efficient sensing system which would help to determine any change in the salinity level to take immediate measures. Some of the impedance measurement systems had been proposed earlier [15], there are disadvantages like low sensitivity, and complicated sensor framework are associated with it. The sensors being developed with MEMS technology, increases its cost of production. Also, these sensors were operated in MHz range which is undesirable in real-time applications.

Flexible materials [17], since their advent, have been a popular choice for sensors over rigid materials. Apart from low fabrication cost and, better mechanical and thermal properties and the ability to conform to curved surfaces are some of the some of the reasons why flexible materials are preferred. Flexible materials have been used for different applications like physiological parameters [18, 19], chemical sensing [20], temperature and humidity sensing [21], environmental monitoring [22], magnetic field detection [23], artificial skins [24], energy harvesting [25, 26], etc. Some of the common polymer substrates used to develop flexible sensors are Polydimethylsiloxane (PDMS) [27], Polyethylene terephthalate (PET) [28], Polyethylene naphthalate (PEN) [29], Polyimide (PI) [30]. Usually, nanoparticles are used to make these materials conductive because of their high surface area, high electrical conductivity, and excellent mechanical properties. The common materials used are carbon [31], graphene [32], gold [33], silver [34], etc. Manufacturing cost per sensor is one of the issues faced during the fabrication of any flexible sensor. This is due to the high value of the equipment or the raw materials used in the process. For example, photolithography [35], which is one of the standard methods employed for developing flexible sensors, has a high equipment cost and requires several steps for the preparation of the sample before the electrodes can be designed on the substrate. It also requires specialized people to handle the raw materials for processing them. Thus, there is interest in the implementation of a technique that is easy to use and enables the development of cheap sensors. Recently, the idea of generating conductive materials from polymers [36] has been approached by the researchers. This is intriguing as it helps to develop sensors at low-cost in a large scale. Graphene, being the conductive material for the fabricated sensors, has certain advantages over other elements. Apart from being one of the highly conductive, it is extremely corrosion resistant [37] which would minimize the effect of oxidation on the electrodes. This paper presents the design and fabrication of laser-induced sensor patches that use the generated graphene as electrodes on commercial tapes. The sensors prototypes were initially tested with different salt concentrations with the idea of developing a fully functionalized sensing system. After validation the functionality of the sensor with a data acquisition system, a microcontroller based sensing system was developed. Figure 1 gives the block diagram of the proposed microcontroller based sensing system. The sensor was controlled by the attached conditioning circuit which processes its output to generate an amplified signal. The development of this system is explained step-by-step in the subsequent sections.

The paper is divided into seven sections. After the introduction given in section one, the fabrication procedure of the sensor patches along with their working principle are explained in sections two and three. The experimental setup and results are given in section four and five respectively, followed by the implementation of a micro-controller based system in section six. Finally, the discussion of the experimental results and conclusion are provided in the final section of the paper.

2. Fabrication of Graphene Sensors

The schematic diagram of the fabrication process of the sensor patches is given in figure 2. Commercial PI films (Zibo Zhongnan Plastics Co., Ltd.) were used as raw materials to develop the sensors. A CO_2 laser system (Model: OLS 6.75 CO_2 laser system, laser spot diameter: 150 microns) was used for the thermal- induction of graphene on the PI films.

The individual fabrication steps are shown in figures 3(a) - 3(d). The polymer film was attached to a glass substrate for support as shown in figure 3(a). CorelDraw software was used to design the electrodes in an interdigitated pattern. Six pairs of electrodes were designed with the length and width of 500 µm and 100 µm, respectively. Figure 3(b) shows the laser induction process of the attached polymer film. The sp^3 hybridized carbon atoms of the polymer film were photo-thermally converted to sp^2 hybridized atoms forming graphene. Power, speed and z-axis were the parameters of the laser system that were optimized for the laser-induced electrode fabrication process. Power (W) determines the amount of energy the laser nozzle operates on. Speed (m/min) refers to the how quickly the nozzle moves over the sample in X-Y directions. Z-axis (mm) determines the focal point of the laser over the sample. This was done by changing the height of the laser platform in the z-direction. The final values used for developing the sensor patches were: Power: 9 watts, speed: 70 m/min, z-axis: 1 mm. The photo-thermally formed graphene was transferred to a Kapton tape with a thickness of 1000 µm. Even though both the ablated film and Kapton tape are made of PI, the reason commercial polymer film were considered as the raw material for laser writing was due to two reasons. Firstly, due to the higher thickness of Kapton tapes, it is not possible to photo-thermally dissolve the sp^3 hybridize carbon atoms of the PI into sp^2 hybridization. This was only possible using thinner films. Secondly, the stickiness of the Kapton tape would have led to the immediate coagulation of the thermally-induced graphene, affecting the design of the electrodes. The placement of the Kapton tape over the induced graphene is shown in figure 3(c). This transfer was done via manual pressure in the vertical direction, all over the tape. The pressure was applied first to the electrode pads and then moving over to the sensing area of the sensor design to make sure of proper adherence of the induced graphene on the Kapton tape. The tape was then pulled off carefully from the PI film to avoid any damage to the transferred graphene. Figure 3(d) shows the sensor patch consisting of transferred conductive material on the Kapton tape. A difference in conductivities of <20 mS/m was observed between the induced and transferred graphene. The front and rear view of the sensor patch is shown in figure 4. The SEM images of the top and cross-sectional views are shown in figures 5(a) and 5(b). It is seen from the images that the edges and electrode lines of the transferred graphene came off clean on the Kapton tape.

3. Working Principle of the Sensor

The electrodes on the sensor patches were designed in an interdigitated pattern. The sensor patch works on capacitive sensing, where one electrode is considered as the excitation one where the voltage was provided, and the other one is considered as a reference electrode. The planar structure of the electrodes provides a non-invasive, in-situ sample measurement technique. Figure 6 shows the working principle for the designed electrodes. When a time-dependent voltage signal is provided to the excitation electrode, an electric field is generated between the oppositely charged electrodes. This field bulges between them due to their planar structure. A one directional measurement condition was provided due to an insulating substrate to the electrodes. The field fringes through any material in contact or proximity to the sensor. This changes the properties of the field which is used [38] to determine the characteristics of the tested material. The penetration depth of the electric field is varied by varying the spatial wavelength (distance between the electrode fingers of the same polarity), which makes it a popular choice for industrial and scientific applications [39, 40].

Electrochemical Impedance Spectroscopy (EIS) was used to analyze the sensor response during the profiling and testing with different salt concentrations. Among the different impedance measurement methods, frequency response analyzer (FRA) was used where the excitation electrode of the sensor was applied with a low amplitude signal as a function of frequency to measure the change in the resulting current. The bonding pads of the sensor were attached to the Kelvin probes to diagnose the changes with the LCR meter. The equivalent circuit regarding electrical parameters was determined using non-linear square curve fitting (CNLS) technique. It uses the electrochemical spectrum analyzer algorithm by making a comparison between the experimental values with the theoretical response. Figures 7 (a) and 7 (b) show the profiling of the sensor in the air and the determination of its equivalent circuit respectively. The change in the response of the sensor patch was studied in terms of real (R) and imaginary (X) part of the impedance (Z). An average of three values was taken from the instrument in order ensure repeatability of its response. These impedance values were fitted into the electrochemical spectrum analyzer to determine the equivalent circuit with respect to the response of the sensor patch in air. Figure 7(b) shows the least square curve fitted Nyquist plot where the circuit is shown in the inset of figure 7(b) gives the equivalent circuit for the similar response as seen from the overlapping theoretical and experimental graphs. The total impendence in the circuit constituted of different components (C_{int}, C_{sol}, and R_{sol}). These individual parameters affect the overall kinetic response of the sensor. C_{sol} and R_{sol} are the solution capacitance and resistance respectively which depends on the properties of the medium. When the solution medium is changed, the conductive properties of the sensor and relative permittivity (ε_r) also changes. This

changes the solution resistance and capacitance. C_{int} is the internal capacitance which arises due to the structure of the electrodes. The internal capacitance also changes when the solution medium is changed. But this change is negligible compared to the changes in the solution capacitance and resistance. The internal capacitance mainly changes by changing the surface area (A) and interdigital distance (d) of the electrodes. The electrode resistance can be considered negligible in this case as the electrodes of the sensor patches are conductive, the change in current due to the resistance (R) would be low. The simulation was carried out with the electrochemical spectrum analyzer with the same range in frequency sweep (1 Hz – 10 kHz) to verify the experimental results with the theoretical one. Table 1 shows the different values along with their error rate, obtained for the electrical parameters in the equivalent circuit. It is seen that the mean square value is in the range of 10^{-2} which suggests an error rate less than 5% [42].

4. Experimental Setup

Sodium Chloride (SA046- 500G) was used as the solute to develop the salt solutions. De-ionized MilliQ® water (Resistance: 18.2 MΩ cm and pH: 6.71) was used as the solvent for the experiments. Serial dilution was performed to develop a series of solutions from 40000 ppm to 4 ppm. Initially, a principal solution of 40000 ppm was prepared by mixing 4 g of solute to 100 ml of solvent. After performing the experiment with this solution, the second solution was prepared by pipetting 10 ml of the principal solution to 90 ml of de-ionized MilliQ® water. This formed 4000 ppm of salt solution. After the second reading, the third solution was formed by pipetting 10 ml of stock solution into 90 ml of de-ionized MilliQ® water to form 400 ppm of salt solution. This process was continued till 4 ppm of salt solution. The experimental setup is shown in figure 8. The experiments were performed with a HIOKI IM 3536 LCR Hi precision tester. The patch was connected to the LCR meter via Kelvin probes for data analysis. The LCR meter was connected to the computer by an USB - USB cable to collect the data in an excel file via an automatic data acquisition algorithm. The sensor patch was fixed to a board with biocompatible tapes (3M Ruban Magique^{MC}) for its stability in water while testing it. The sensing area of the patch was carefully immersed into the solution to make sure that bonding pads of the sensor and the connected probes do not come in contact with the solution. After each experiment, the sensor patch was thoroughly washed with MilliQ® water and dried in the oven for 10 minutes before re-using it for the next experiment. A sinusoidal signal with a fixed voltage of 1 V peak-to-peak was applied from the LCR meter, and the frequency was swept from 1 Hz to 10 kHz. The resistance (R) and reactance (X) was calculated from the LCR meter.

5. Experimental Results

The response of the sensor patch to the tested samples is shown in figures 9 and 10 in terms of resistance (R) and reactance (X) respectively. It is seen that the sensor patch is distinctively sensitive towards the different tested salt concentrations. Even though it is seen that from figure 9 shows that the resistance changes symmetrically for all the tested solutions, the change in reactance as seen from figure 10 is prominent only within a certain range. The resistance decreases with the increase in the salt concentration due to the increase in ionic current passing through the circuit. The frequency of operation had a major role to play for the change in reactance compared to the change in resistance. For the change in reactance, the frequency range between 0.4093 kHz – 7.152 kHz displays a prominent change for different concentrations. The reactance changes as a result of the capacitive part of the sensor which depends on both the frequency and concentration of the sample. The changes in the response for the reactance occur due to the faradic currents going through the tested sample. Figure 10 shows the Nyquist plot between the real and imaginary part of the impedance. The readings shown in the Nyquist plot also shows a clear distinction between the different test concentrations. This plot is different from figure 7(a) that was obtained during the profiling of the sensor in air. These changes occur as a result of the changes in the elements constituting the equivalent circuit.

A particular frequency (4.205 kHz) was chosen from the sensitive region to develop the characteristic curve as shown in figure 12. The chosen frequency depicted highest difference in the experimental values for the salt concentrations. The sensitivity of the sensor patch was also calculated for the given solutions. Figure 13 shows the sensitivity values for different salt concentrations. The highest sensitivity value obtained by these sensors was around 1.07 Ω/ppm. This is more than all the sensitivity values of the salinity sensors reported by the researchers in their earlier work where the sensors were developed with polymer [3], interferometer [43] and fiber optic probes [44]. The sensitivity values were calculated based on equation (1).

$$= \frac{\Delta}{\Delta} \quad (1)$$

A real time sample of unknown concentration was considered for testing to validate the developed system. After performing a frequency sweep between 1 Hz to 10 kHz, the response of the sensor towards the same frequency value was considered which was used to develop the standard and sensitivity curve. The measured values of the tested sample at that frequency (4.205 kHz) were: Resistance (R): 1738.35 Ω, reactance (X): 901.486 Ω. Substituting the resistance value to the equation obtained from the standard curve,

$$= 5 \quad 10^{-2} \quad ( ) + 1651.7 \quad (2)$$

$$1738.35 = 0.005 \quad ( ) + 1651.7 \quad (3)$$

$$= \frac{1738.35 - 1651.7}{0.005} \quad (4)$$

$$= 35330 \quad (5)$$

The experimental value of the real sample was 35330 ppm. This was cross-checked with a refractometer; a standard device used to determine the salinity level of the real samples in the marine and biological industries [45, 46]. The actual concentration of this sample was 35000 ppm. This proved our experimental value to be very close to the actual value. The error rate calculated from this sample measurement was 0.9%. Figure 14 shows the equivalent circuit for the Nyquist plot developed from the experimental values after the sensor. It is seen from figures 7 and 14 that there is a change in the components of the equivalent circuit. A constant phase element (CPE) has been added in series with the internal capacitor of the sensor. The constant, n, is close to 1, which proves that the behavior of the CPE resembles that of a capacitor. The presence of CPE in the circuit is defined as the adsorption capacitance (C_{ad}). This C_{ad} arises due to the ion diffusion process between the sensing surface of the electrode and the bulk solution [47]. The solution capacitance (C_{sol}) and resistance (R_{sol}) are two important parameters to determine the change in response of the system kinetics. Table 2 presents the different parameters along with their values and error rate. It is seen that the error rate for each of the elements in the generated equivalent circuit is less than 5% [48]. Figure 15 shows the response of the sensor towards the change in temperature in terms of resistance values. The measurement of the five concentrations was taken at five temperature values (10°C - 50°C) at the chosen frequency (4.205 kHz). It is seen that the changes in resistance is negligible with the changes in temperature for each concentration. Figure 16 shows the repeatability of the sensor responses where experiments with each concentration were carried out six times with duration of two hours between each experiment. It is seen from the response that the difference between the sensor responses towards each concentration for the six cases is very negligible and the deviation from the mean value lies below 2%.

In order to develop a sensing system, the same frequency value (4.205 kHz) was fixed in the microcontroller to determine if the change in the concentration of the solution can be determined by the embedded system. A conditioning circuit was developed with the microcontroller before testing the sensor with solutions of same concentrations.

6. Microcontroller Based Sensing System

Arduino Uno and Arduino Integrated Development Environment (IDE) were used as the microcontroller (μC) device and the associated software, respectively, to test the sensor patch for different salt concentrations. Figure 17 shows the block diagram regarding the connection of the sensor to the microcontroller. The sensor output was passed through a buffer and a low-pass filter to the microcontroller. The operating voltage fed to the microcontroller was fixed at 3.3 V. Followed by providing a sinusoidal voltage signal to the sensor, the output was passed through an amplifier circuit. This consisted of a buffer and an active low-pass filter. This was done to transfer the maximum response of the sensor by reducing the noise and amplifying the signal. The schematic diagram of the sensor with the amplifying circuit is shown in figure 18. The non-inverting gain provided to the output signal from the sensor was 23. This was done to have an amplified response of the output voltage from the sensor occurring due to the difference in salt concentrations. The output of the low-pass filter was used as the analog input to the microcontroller's analog-to-digital converter. Figure 19 shows the voltage readings for the measured concentrations. It is seen from the figure that the response of the sensor changes almost linearly with the change in concentration. This suggests that the signal conditioned microcontroller is capable of

detecting the small changes happening in the solution. The ultimate motive is to develop a system to give a full-scale voltage during the real-time testing of sea water samples. The microcontroller based system would be useful in real-life situations where the system, apart from the sensing surface of the sensor patch, can be capsuled inside a waterproof case to examine the changes in salinity in the water.

7. Discussion and Conclusion

The paper showcases the development of a sensing system for the detection of different salt concentrations in the water bodies. The main motive to develop this system was to deal with the problems faced by flora and fauna existing inside the water bodies. Pulsed laser irradiated graphene sensor patches were developed based on the transfer of laser-induced graphene to commercial sticky tapes, providing cheap, flexible and corrosion resistance electrodes. The cost of production of the sensor prototypes was cheap as a single step fabrication was done from low-cost commercial PI films. The films are highly flexible due to the low tensile stress (2.5 GPa) [49]. The sensor patches were highly conductive (200 mS) with a high sensitivity (1.07 Ω/ppm) and a resolution of 1 ppm for the tested salt samples. One of the biggest advantages of these sensors is the biocompatibility of the material used to develop the electrodes. This would minimize the effects caused by other metallic electrode systems used for the similar applications. But, there are some issues that need to be resolved before implementing the proposed system for real-time applications. Firstly, apart from sodium chloride, there are other molecular constituents present in sea water. This can affect the sensor response in real-time applications. This can be resolved by attaining selectivity towards the chosen molecule. Secondly, the response of the sensor can also be influenced by elements having ionic properties similar to sodium and chloride ions. The similarity in properties arises mainly from the similarity in structure, density, and electron affinity. The problem of similarity occurs especially with salts comprising of sodium as the cation. This would mislead the monitoring unit, thus generating erroneous results. These problems are to be addressed and report in near future work in the process of developing a low cost, fully-functionalized salinity measurement system.

Acknowledgement

The authors would like to thank King Abdullah University of Science and Technology, Saudi Arabia, for providing the conditions to test the sensor patch and facilities for fabrication of the electrodes respectively. They would also thank the Macquarie University, Australia for providing the conditions to perform experiments with the developed sensor patches.

References

[1] Natural environment. Available at http://www.environment.nsw.gov.au/salinity/basics/naturalenvironment.htm. Last accessed on 23.07.2017.
[2] Changes in Marine Salinity Levels. Available at http://pisaster.genetics.uga.edu/groups/evolution3000/wiki/cb536/Changes_in_Marine_Salinity_Levels.html. Last accessed on 23.07.2017
[3] C. Wu, B.-O. Guan, C. Lu, H.-Y. Tam, Salinity sensor based on polyimide-coated photonic crystal fiber, Optics express, 19(2011) 20003-8.
[4] S. Robinson, R. Nakkeeran, Photonic crystal based sensor for sensing the salinity of seawater, Advances in Engineering, Science and Management (ICAESM), 2012 International Conference on, IEEE2012, pp. 495-9.
[5] S. Wang, J. Wang, G. Li, L. Tong, Modeling optical microfiber loops for seawater sensing, Applied optics, 51(2012) 3017-23.
[6] H.A. Rahman, S.W. Harun, M. Yasin, H. Ahmad, Fiber-optic salinity sensor using fiber-optic displacement measurement with flat and concave mirror, IEEE Journal of selected topics in quantum electronics, 18(2012) 1529-33.
[7] Murray-Darling Basin Authority annual report 2015-16.
[8] C. Huber, I. Klimant, C. Krause, T. Werner, T. Mayr, O.S. Wolfbeis, Optical sensor for seawater salinity, Fresenius' journal of analytical chemistry, 368(2000) 196-202.
[9] N. Reul, S. Fournier, J. Boutin, O. Hernandez, C. Maes, B. Chapron, et al., Sea surface salinity observations from space with the SMOS satellite: A new means to monitor the marine branch of the water cycle, Surveys in Geophysics, 35(2014) 681-722.
[10] L. Men, P. Lu, Q. Chen, A multiplexed fiber Bragg grating sensor for simultaneous salinity and temperature measurement, Journal of Applied Physics, 103(2008) 053107.
[11] D. Gadani, V. Rana, S. Bhatnagar, A. Prajapati, A. Vyas, Effect of salinity on the dielectric properties of water, (2012).
[12] D.M. Le Vine, G.S. Lagerloef, S.E. Torrusio, Aquarius and remote sensing of sea surface salinity from space, Proceedings of the IEEE, 98(2010) 688-703.
[13] H. Rahman, S. Harun, M. Yasin, S. Phang, S. Damanhuri, H. Arof, et al., Tapered plastic multimode fiber sensor for salinity detection, Sensors and Actuators A: Physical, 171(2011) 219-22.
[14] E. Scudiero, A. Berti, P. Teatini, F. Morari, Simultaneous monitoring of soil water content and salinity with a low-cost capacitance-resistance probe, Sensors, 12(2012) 17588-607.
[15] J. Jonsson, K. Smedfors, L. Nyholm, G. Thornell, Towards chip-based salinity measurements for small submersibles and biologgers, International Journal of Oceanography, 2013(2013).
[16] S. Bhat, Salinity (conductivity) sensor based on parallel plate capacitors, (2005).
[17] W.S. Wong, A. Salleo, Flexible electronics: materials and applications: Springer Science & Business Media; 2009.
[18] A. Nag, S.C. Mukhopadhyay, J. Kosel, Tactile Sensing From Laser-Ablated Metallized PET Films, IEEE Sensors Journal, 17(2016) 7-13.
[19] A. Nag, S.C. Mukhopadhyay, J. Kosel, Flexible carbon nanotube nanocomposite sensor for multiple physiological parameter monitoring, Sensors and Actuators A: Physical, 251(2016) 148-55.
[20] M.E. Roberts, S.C. Mannsfeld, R.M. Stoltenberg, Z. Bao, Flexible, plastic transistor-based chemical sensors, Organic Electronics, 10(2009) 377-83.
[21] A. Oprea, J. Courbat, N. Bârsan, D. Briand, N. De Rooij, U. Weimar, Temperature, humidity and gas sensors integrated on plastic foil for low power applications, Sensors and Actuators B: Chemical, 140(2009) 227-32.
[22] D. Briand, A. Oprea, J. Courbat, N. Bârsan, Making environmental sensors on plastic foil, Materials Today, 14(2011) 416-23.
[23] B. Li, M.N. Kavaldzhiev, J. Kosel, Flexible magnetoimpedance sensor, Journal of Magnetism and Magnetic Materials, 378(2015) 499-505.
[24] A. Alfadhel, J. Kosel, Magnetic nanocomposite cilia tactile sensor, Advanced Materials, 27(2015) 7888-92.
[25] M.T. Ghoneim, M.A. Zidan, M.Y. Alnassar, A.N. Hanna, J. Kosel, K.N. Salama, et al., Thin PZT-Based Ferroelectric Capacitors on Flexible Silicon for Nonvolatile Memory Applications, Advanced electronic materials, 1(2015).
[26] M.Y. Alnassar, Y.P. Ivanov, J. Kosel, Flexible Magnetoelectric Nanocomposites with Tunable Properties, Advanced electronic materials, 2(2016).
[27] S. Khan, S. Tinku, L. Lorenzelli, R.S. Dahiya, Flexible tactile sensors using screen-printed P (VDF-TrFE) and MWCNT/PDMS composites, IEEE Sensors Journal, 15(2015) 3146-55.
[28] U. Yaqoob, D.-T. Phan, A.I. Uddin, G.-S. Chung, Highly flexible room temperature NO 2 sensor based on MWCNTs-WO 3 nanoparticles hybrid on a PET substrate, Sensors and Actuators B: Chemical, 221(2015) 760-8.
[29] Y. Zang, F. Zhang, C.-a. Di, D. Zhu, Advances of flexible pressure sensors toward artificial intelligence and health care applications, Materials Horizons, 2(2015) 140-56.
[30] J.A. Dobrzynska, M.A. Gijs, Flexible polyimide-based force sensor, Sensors and Actuators A: Physical, 173(2012) 127-35.
[31] H.Y. Jeong, D.-S. Lee, H.K. Choi, D.H. Lee, J.-E. Kim, J.Y. Lee, et al., Flexible room-temperature NO 2 gas sensors based on carbon nanotubes/reduced graphene hybrid films, Applied Physics Letters, 96(2010) 213105.
[32] Y.H. Kwak, D.S. Choi, Y.N. Kim, H. Kim, D.H. Yoon, S.-S. Ahn, et al., Flexible glucose sensor using CVD-grown graphene-based field effect transistor, Biosensors and Bioelectronics, 37(2012) 82-7.
[33] S. Gong, W. Schwalb, Y. Wang, Y. Chen, Y. Tang, J. Si, et al., A wearable and highly sensitive pressure sensor with ultrathin gold nanowires, Nature communications, 5(2014).
[34] L. Hu, H.S. Kim, J.-Y. Lee, P. Peumans, Y. Cui, Scalable coating and properties of transparent, flexible, silver nanowire electrodes, ACS nano, 4(2010) 2955-63.
[35] N. Herzer, S. Hoeppener, U.S. Schubert, Fabrication of patterned silane based self-assembled monolayers by photolithography and surface reactions on silicon-oxide substrates, Chemical Communications, 46(2010) 5634-52.
[36] J. Lin, Z. Peng, Y. Liu, F. Ruiz-Zepeda, R. Ye, E.L. Samuel, et al., Laser-induced porous graphene films from commercial polymers, Nature communications, 5(2014).
[37] Graphene paints a corrosion-free future. Available at http://www.manchester.ac.uk/discover/news/graphene-paints-a-corrosion-free-future. Last accessed on 23.07.2017.
[38] S.C. Mukhopadhyay, C.P. Gooneratne, A novel planar-type biosensor for noninvasive meat inspection, Sensors Journal, IEEE, 7(2007) 1340-6.
[39] S.C. Mukhopadhyay, C.P. Gooneratne, G.S. Gupta, S.N. Demidenko, A low-cost sensing system for quality monitoring of dairy products, IEEE Transactions on Instrumentation and Measurement, 55(2006) 1331-8.
[40] M.S.A. Rahman, S.C. Mukhopadhyay, P.-L. Yu, J. Goicoechea, I.R. Matias, C.P. Gooneratne, et al., Detection of bacterial endotoxin in food: New planar interdigital sensors based approach, Journal of Food Engineering, 114(2013) 346-60.

[41] M.S.A. Rahman, S.C. Mukhopadhyay, P.-L. Yu, Novel Planar Interdigital Sensors, Novel Sensors for Food Inspection: Modelling, Fabrication and Experimentation, Springer2014, pp. 11-35.
[42] EIS Spectrum Analyzer. Available at http://www.abc.chemistry.bsu.by/vi/analyser/. Last accessed on 23.07.2017.
[43] C. Wu, H. Fu, H. Au, B.-O. Guan, H. Tam, High-sensitivity salinity sensor realized with photonic crystal fiber Sagnac interferometer, 21st International Conference on Optical Fibre Sensors (OFS21), International Society for Optics and Photonics2011, pp. 77531B-B-4.
[44] N. Diaz-Herrera, O. Esteban, M. Navarrete, M. Le Haitre, A. González-Cano, In situ salinity measurements in seawater with a fibre-optic probe, Measurement Science and Technology, 17(2006) 2227.
[45] D. Malarde, Z.Y. Wu, P. Grosso, J.d.B. de la Tocnaye, M. Le Menn, High-resolution and compact refractometer for salinity measurements, Measurement Science and Technology, 20(2008) 015204.
[46] P. Grosso, M. Le Menn, J.-L.D.B. De La, Z.Y. Wu, D. Malardé, Practical versus absolute salinity measurements: New advances in high performance seawater salinity sensors, Deep Sea Research Part I: Oceanographic Research Papers, 57(2010) 151-6.
[47] A.V. Mamishev, K. Sundara-Rajan, F. Yang, Y. Du, M. Zahn, Interdigital sensors and transducers, Proceedings of the IEEE, 92(2004) 808-45.
[48] M.S.A. Rahman, S.C. Mukhopadhyay, P.-L. Yu, Experimental Investigation: Impedance Characterization, Novel Sensors for Food Inspection: Modelling, Fabrication and Experimentation, Springer2014, pp. 37-71.
[49] Kapton properties. Available at http://www.dupont.com/content/dam/dupont/products-and-services/membranes-and-films/polyimde-films/documents/DEC-Kapton-summary-of-properties.pdf. Last accessed on 23.07.2017.

Mr. Anindya Nag has completed his Bachelor of Technology degree in Electronics and Communication from West Bengal Institute of Technology, India in 2013 and received his Master of Engineering (M.E.) degree from Massey University, New Zealand in June 2015. His major during his M.E. degree was Electronics and Computer Systems. His research interests are in the area of Smart Sensors and Sensing Technology for home and environmental monitoring. He is currently pursuing Ph.D. in Faculty of Engineering at Macquarie University, Australia and is working on Printed Flexible Sensors for Human Wellness.

Dr. Subhas Chandra Mukhopadhyay (M'97, SM'02, F'11) graduated from the Department of Electrical Engineering, Jadavpur University, Calcutta, India with a Gold medal and received the Master of Electrical Engineering degree from Indian Institute of Science, Bangalore, India. He has Ph.D. (Eng.) degree from Jadavpur University, India and Doctor of Engineering degree from Kanazawa University, Japan. Currently, he is working as a Professor of Mechanical/Electronics Engineering with the Department of Engineering, Macquarie University, New South Wales, Australia. He is the Program Leader of the Mechatronics Engineering Degree Program. He has over 26 years of teaching and research experiences. His fields of interest include Smart Sensors and Sensing Technology, Wireless Sensor Networks, Instrumentation and Measurements, Internet of Things, Environmental Measurements, Electromagnetics, Control Engineering, Mechatronics, Magnetic Bearing, Fault Current Limiter, Electrical Machines and numerical field calculation, etc. He has authored/co-authored over 400 papers in different international journals, conferences and book chapter. He has edited fifteen conference proceedings. He has also edited seventeen special issues of international journals as lead guest editor and thirty books with Springer-Verlag. He was awarded numerous awards throughout his career and attracted over US$3.0 M on different research projects. He has delivered 296 seminars including keynote, tutorial, invited and special seminars. He is a Fellow of IEEE (USA), a Fellow of IET (UK) and a Fellow of IETE (India). He is a Topical Editor of IEEE Sensors Journal and an Associate Editor IEEE Transactions on Instrumentation and Measurements. He is on the editorial board of e-Journal on Non-Destructive Testing, Sensors and Transducers, Transactions on Systems, Signals and Devices (TSSD). He is the co-Editor-in-chief of the International Journal on Smart Sensing and Intelligent Systems (www.s2is.org). He was the Technical Program Chair of ICARA 2004, ICARA 2006, ICARA 2009 and IEEE I2MTC 2016. He was the General chair/co-chair of ICST 2005, ICST 2007, IEEE ROSE 2007, IEEE EPSA 2008, ICST 2008, IEEE Sensors 2008, ICST 2010, IEEE Sensors 2010, ICST 2011, ICST 2012, ICST 2013, ICST 2014, ICST 2015 and ICST 2016. He has organized the IEEE Sensors Conference 2009 at Christchurch, New Zealand during October 25 to 28, 2009 as the General Chair. He is currently organizing the 11th ICST in Sydney, Australia during December 4-6, 2017, (http://www.cvent.com/d/nvqbb9). He is the Ex-Chair of the IEEE Instrumentation and Measurement Society New Zealand Chapter. He is a Distinguished Lecturer of IEEE Sensors Council from 2017-2019.

Dr. Jurgen Kosel has received his Dipl.-Ing. (M.Sc.) and Ph.D. degrees in Electrical Engineering from the Vienna University of Technology, Vienna, Austria, in 2002 and 2006, respectively. From 2006 to 2007, he worked in the automotive industry as a Project Manager with Magna Powertrain, Graz, Austria. He was a post-doctoral fellow at the Biomedical Engineering Research Group, Stellenbosch University, South Africa, from 2007 to 2009. Currently, he is an Associate Professor of Electrical Engineering at the King Abdullah University of Science and Technology (KAUST), Thuwal, Saudi Arabia. He is the head of the Sensing, Magnetism, and Microsystems Research Group. His research interests are in the fields of micro and nano devices with a focus on magnetic transducers.

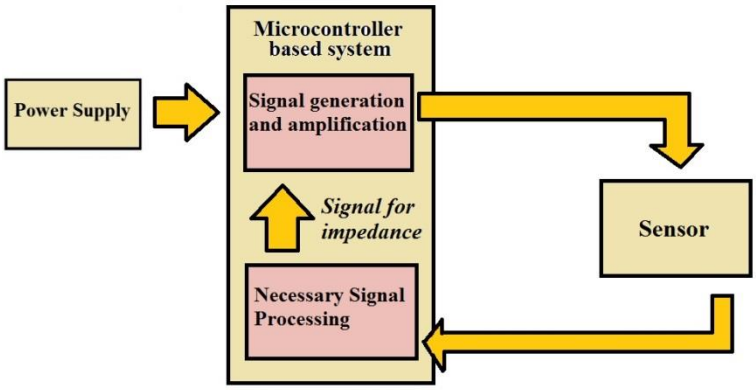

Fig. 1: Block diagram for the proposed microcontroller based sensing system for salinity measurement.

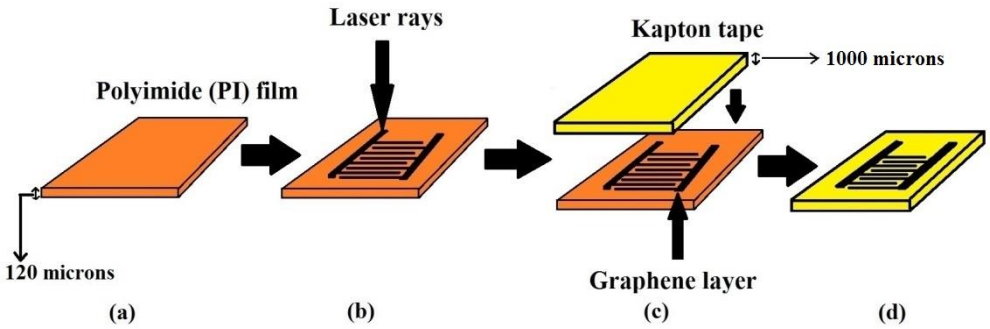

Fig. 2: Schematic diagram of the steps of fabrication of the graphene sensor. (a) The polyimide film, with a thickness of around 120 µm, is taken as the substrate material for laser writing process. (b) The laser writing was done on the film. (c) The thermally-induced material is shifted manually by compressing it against the generated graphene. (d) The final sensor prototype.

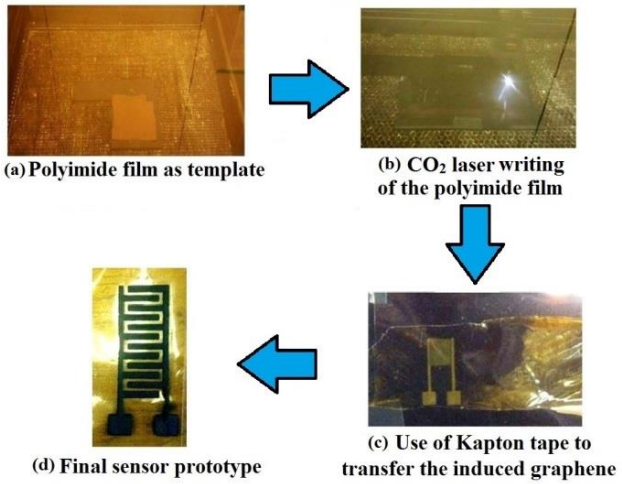

Fig. 3: Fabrication steps of the sensor.

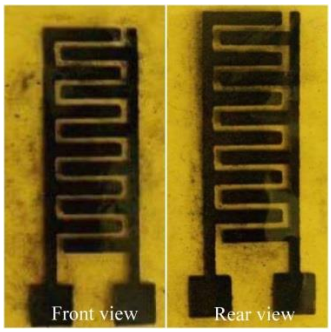

Fig. 4: Front and rear view of the sensor patch.

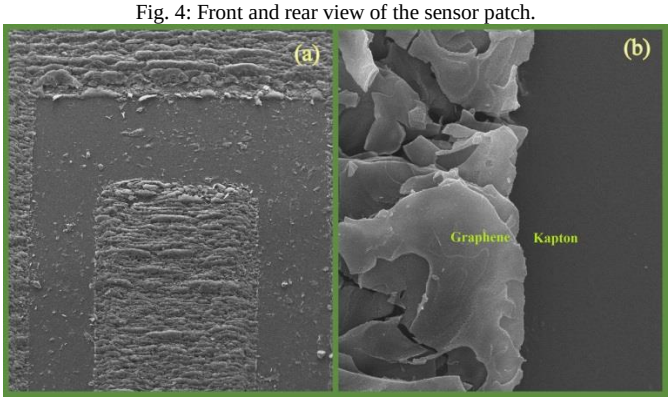

Fig. 5: SEM image of the (a) Top view of an electrode finger of the sensor patch (b) Zoom top-view showing the electrode lines.

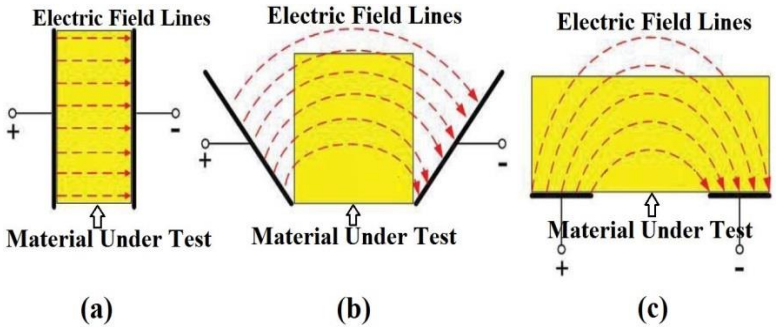

Fig. 6: Working principle of developed sensor electrodes. (a) The idea of parallel plate capacitor is used as the structure for the electrodes. (b) Electric field lines are generated between the oppositely charged electrodes. Due to the planar structure of the electrodes, the field lines bulge from one electrode to another (c) The field lines penetrates through any material kept in contact or proximity [41].

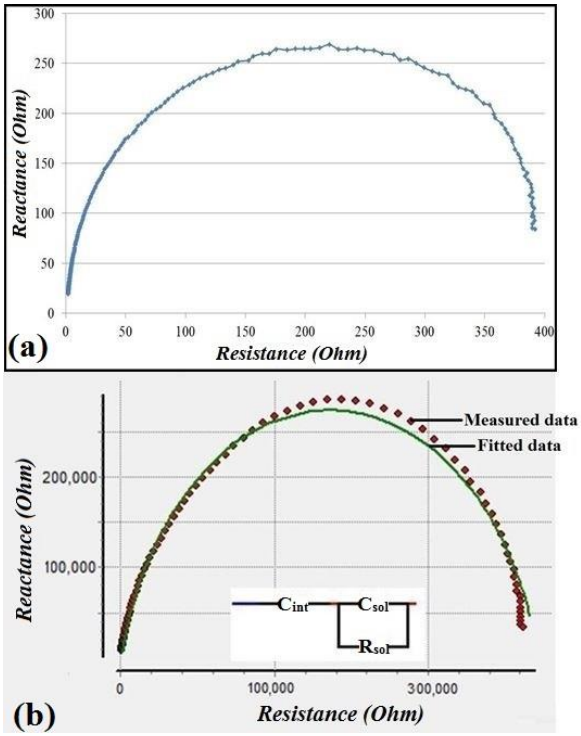

Fig. 7: (a) Profiling of the sensor done in air. (b) Least square curve fitting plot for Nyquist plot. The red dots determine the experimental data with the green line being the fitted curve.

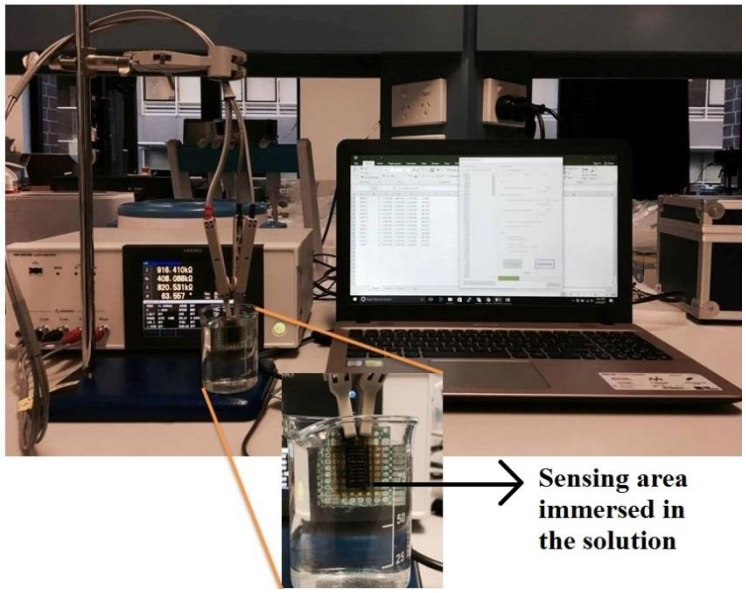

Fig. 8: Experimental setup showing the attachment of the sensor patch to the LCR meter via Kelvin probes. The sensing area of the patch was immersed in the solution. The LCR meter was connected to the laptop to collect the data.

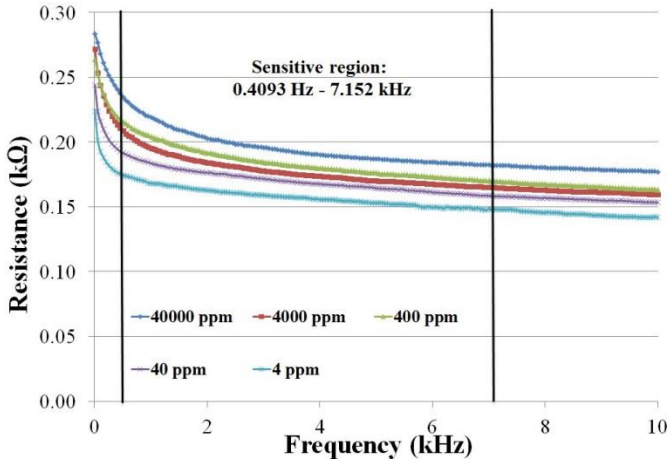

Fig. 9: Response of the sensor patch for different concentrations of salt in terms of resistance and frequency.

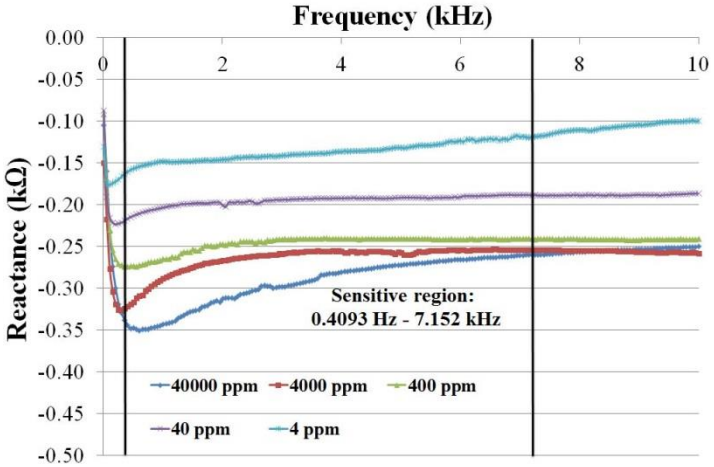

Fig. 10: Response of the sensor patch for different concentrations of salt in terms of reactance and frequency.

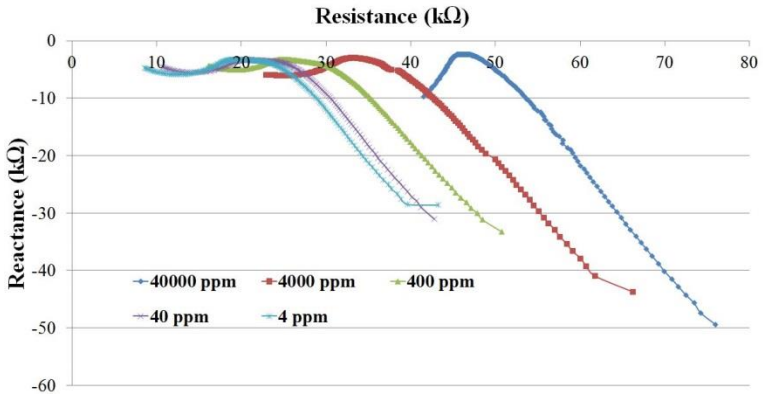

Fig. 11: Response of the sensor patch for different concentrations of salt in terms of Nyquist plot.

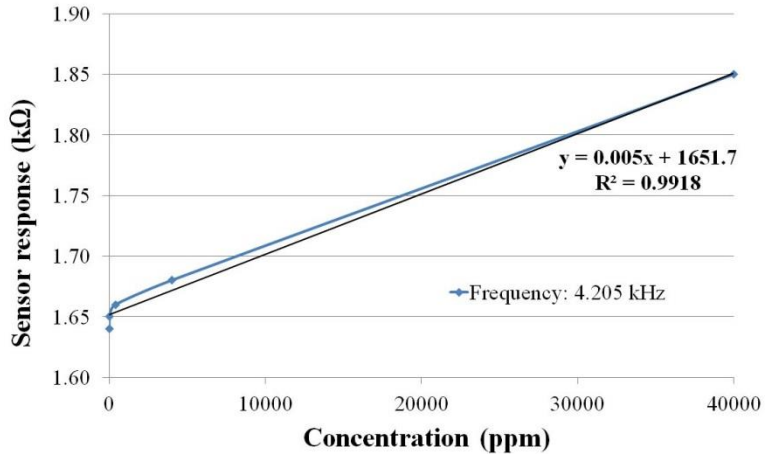

Fig. 12: Standard curve for different experimental concentrations.

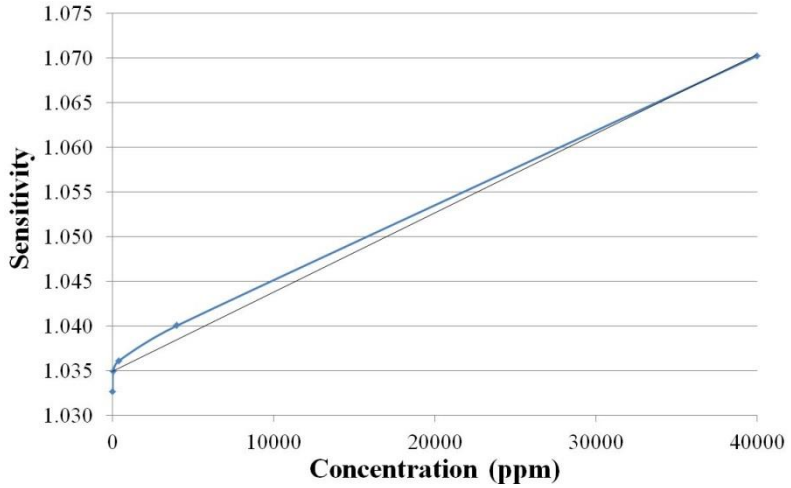

Fig. 13: Sensitivity curve for different solutions.

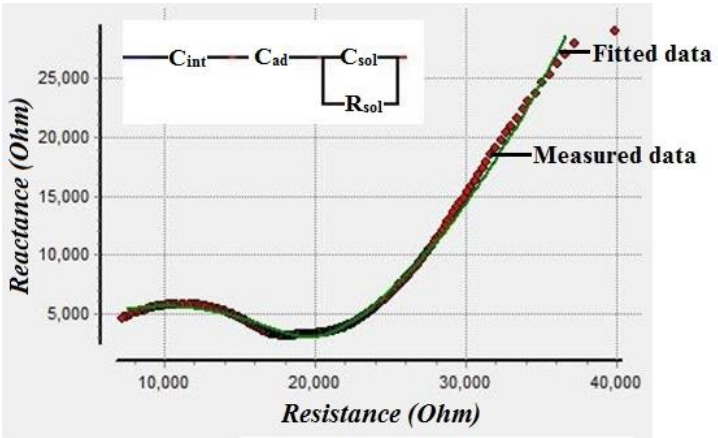

Fig. 14: Least square curve fitting for Nyquist plot with the experimental data.

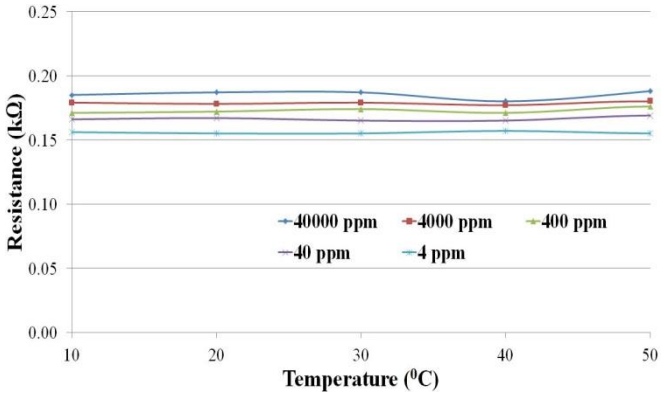

Fig. 15: Dependence of the sensor response towards the temperature for different salt concentrations.

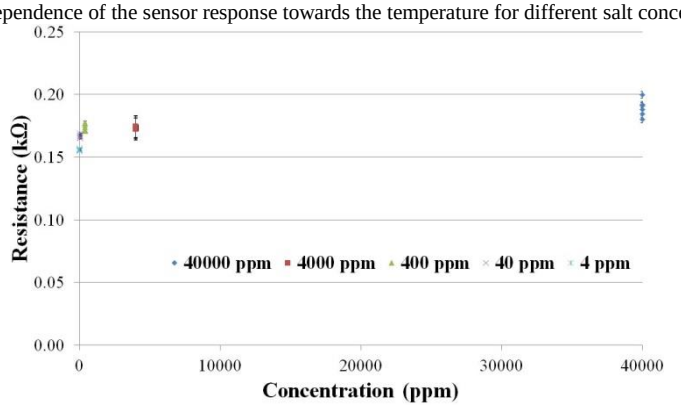

Fig. 16: Repeatability of the sensor response illustrated with six experiments with each salt concentration.

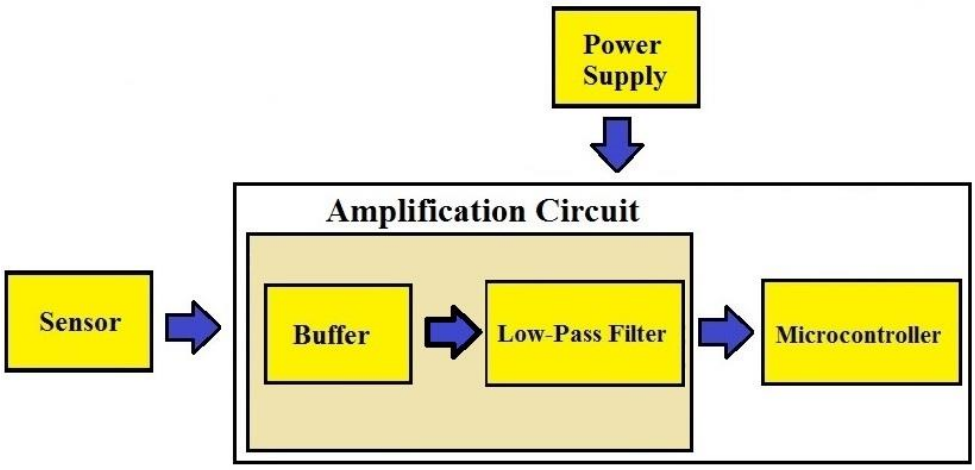

Fig. 17: Block diagram depicting the connection of the sensor to the microcontroller. The buffer and low-pass filter were added to the circuitry for a proper analysis of the output from the sensor.

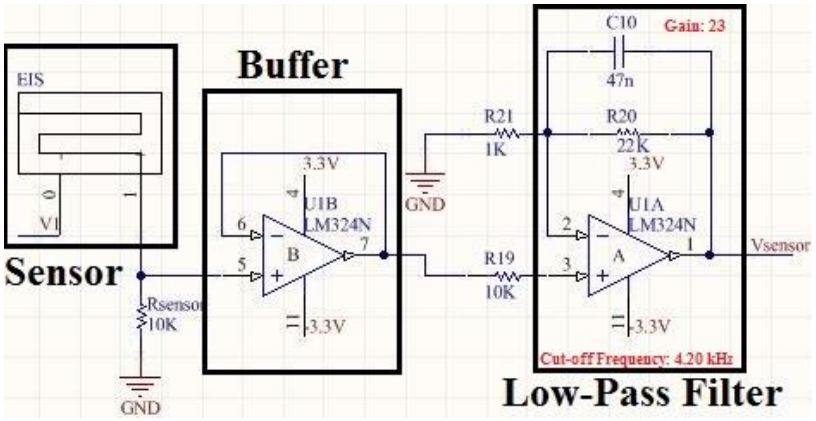

Fig. 18: Circuit design for the conditioning circuit used to process the sensor output before feeding it to the microcontroller.

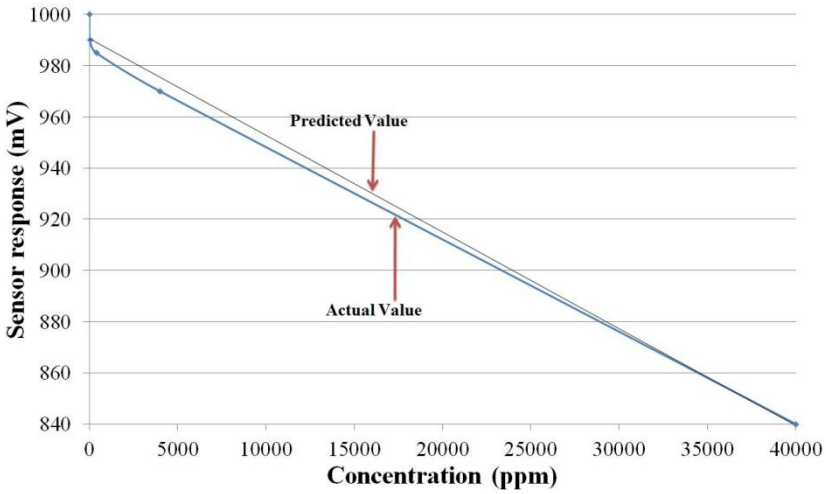

Fig. 19: Response of the microcontroller for different salt concentrations.

Table 1: Equivalent circuit parameters (as shown in the inset of Fig. 7(b)) along with their results and error %.

Equivalent circuit electrical parameters	**Result**	**Error%**	**r^2 (amplitude)**
C_{int} (pF)	71.22	1.945	0.036965
C_{sol} (pF)	8.99	0.8149	
R_{sol} (kΩ)	343	4.0456	

Table 2: Equivalent circuit parameters along with their limits, result and error % to determining the fitted curve on the experimental data.

Equivalent circuit electrical parameters	**Result**	**Error%**	**r^2 (amplitude)**
C_{sol} (µF)	1.171	2.462	0.000614
R_{sol} (kΩ)	18.6	0.4922	
C_{int} (µF)	6.8	0.9457	
N	0.84244	0.3808	
C_{ad} (µF)	113	2.526	